CELL BIOLOGY

Cardiac cell–integrated microneedle patch for treating myocardial infarction

Junnan Tang[1,2,3], Jinqiang Wang[3], Ke Huang[2,3], Yanqi Ye[3], Teng Su[2,3], Li Qiao[2,3,4], Michael Taylor Hensley[2,3], Thomas George Caranasos[5], Jinying Zhang[1], Zhen Gu[3,6,7]*, Ke Cheng[1,2,3,8]*

We engineered a microneedle patch integrated with cardiac stromal cells (MN-CSCs) for therapeutic heart regeneration after acute myocardial infarction (MI). To perform cell-based heart regeneration, cells are currently delivered to the heart via direct muscle injection, intravascular infusion, or transplantation of epicardial patches. The first two approaches suffer from poor cell retention, while epicardial patches integrate slowly with host myocardium. Here, we used polymeric MNs to create "channels" between host myocardium and therapeutic CSCs. These channels allow regenerative factors secreted by CSCs to be released into the injured myocardium to promote heart repair. In the rat MI model study, the application of the MN-CSC patch effectively augmented cardiac functions and enhanced angiomyogenesis. In the porcine MI model study, MN-CSC patch application was nontoxic and resulted in cardiac function protection. The MN system represents an innovative approach delivering therapeutic cells for heart regeneration.

INTRODUCTION

On average, 635,000 Americans have a new coronary heart attack per year, which is defined as the first instance of a hospitalized myocardial infarction (MI) or a coronary heart disease death. Around 300,000 more have a recurrent attack, and an additional 155,000 experience silent MIs (*1*). Thirty-six percent of MI survivors will have an increased risk of developing heart failure down the road (*2*, *3*). To date, no approved therapy has been developed to decrease the size of an established heart scar (*4*). Stem cell therapy aims to improve the treatment options available to MI survivors. It seeks to curb adverse heart remodeling, to regenerate viable myocardium, and to reduce scar size (*5*). In the past two decades, stem cell therapies have gained attention as potential therapies for many incurable diseases (*6*–*8*). Paracrine mechanism plays an essential role in adult stem cell–mediated tissue repair. For example, regenerative factors released from stem cells can promote endogenous repair of the injured myocardium (*9*–*11*). We have been studying heart-derived cardiac stem/stromal cells (CSCs) over the past several years (*12*–*14*). The notion that injection of CSCs may offer beneficial effect since mild to moderate MI has been confirmed in recently completed clinical trials (*15*, *16*). One major hurdle hampering the efficacy of CSC therapy is the extremely low cell retention rate after delivery (*17*). Within 24 hours of delivery, more than 90% of injected cells are typically lost (*18*, *19*), regardless of the delivery route (such as intracoronary or intramyocardial injection). Bioengineering approaches, including injectable biomaterials, cardiac patches, and magnetic/molecular targeting, have been studied to improve cell engraftment rate (*20*). The cardiac patch strategy can drastically improve cell retention (*21*). However, the challenge remains to integrate the transplanted biomaterials/stem cells construct with the host myocardium. Previous reports indicated that integration happened slowly (*22*).

Here, we described a polymeric microneedle patch integrated with CSCs (MN-CSCs) for therapeutic heart regeneration. The painless MN patches have been established as an effective transcutaneous delivery device for transporting a variety of therapeutics (*23*–*28*). In this strategy, the MN-CSC system offers unique advantages over conventional cardiac patches: The MNs serve as the channels to allow for communication between the patch and the host myocardium, as the transplanted patch could get nutrients from the heart while releasing the paracrine factors to repair the heart. We demonstrated that the MN-CSC patch could promote healing in experimental animals of MI by promoting angiomyogenesis, reducing scar size, and augmenting cardiac functions.

RESULTS

Characterization of MN array

The concept of MN-CSC cardiac patch therapy is illustrated in Fig. 1A. Briefly, a MN patch was fabricated from an aqueous solution of biocompatible polymer poly(vinyl alcohol) (PVA) via a micromolding approach (*23*). The PVA is 99% hydrolyzed and has a molar mass of 89,000 to 98,000 g/mol. The prepared MN array patch was a 12-mm by 12-mm patch with a 20 by 20 MN array. The needle had a conical shape, with a base diameter of 300 μm, a tip diameter of 5 μm, and a height of 600 μm, as confirmed by scanning electron microscopy (SEM) and fluorescence microscopy (Fig. 1B and fig. S1A). The MN had a mechanical strength of ~2 N per needle (fig. S1B), which allowed for sufficient skin penetration without breaking (*29*, *30*). Meanwhile, the integrity of the PVA MN was maintained without obvious deformation in phosphate-buffered saline (PBS) during days 1, 3, and 7 (fig. S1C).

Biocompatibility of the MN array with CSCs and cardiomyocytes

Rat CSCs (1×10^5) were encapsulated in the fibrin gel and then integrated onto the surface of MN array (Fig. 1C). The porous structure of MN allowed the release of CSC factors through the polymeric needles. The integrated MN-CSC patch was cultured by positioning

[1]Department of Cardiology, The First Affiliated Hospital of Zhengzhou University, Zhengzhou, Henan 450052, China. [2]Department of Molecular Biomedical Sciences and Comparative Medicine Institute, North Carolina State University, Raleigh, NC 27607, USA. [3]Joint Department of Biomedical Engineering, University of North Carolina at Chapel Hill and North Carolina State University, Raleigh, NC 27607, USA. [4]Department of Cardiology, The Second Affiliated Hospital of Hebei Medicial University, Shijiazhuang, Hebei 050000, China. [5]Division of Cardiothoracic Surgery, University of North Carolina at Chapel Hill, Chapel Hill, NC 27599, USA. [6]Department of Bioengineering, University of California, Los Angeles, CA, USA. [7]California NanoSystems Institute, Center for Minimally Invasive Therapeutics, University of California, Los Angeles, CA, USA. [8]Division of Pharmacoengineering and Molecular Pharmaceutics, Eshelman School of Pharmacy, University of North Carolina at Chapel Hill, Chapel Hill, NC 27599, USA.
*Corresponding author. Email: ke_cheng@ncsu.edu (K.C.); guzhen@ucla.edu (Z.G.)

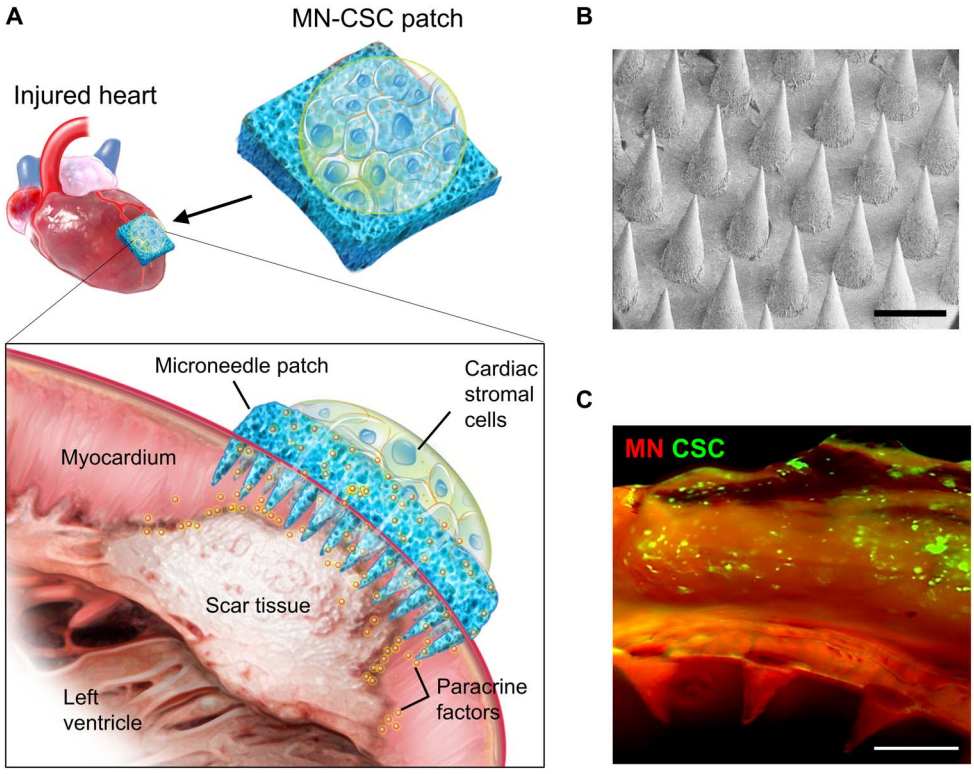

Fig. 1. Characterization of MN-CSCs. (**A**) Schematic showing the overall design used to test the therapeutic benefits of MN-CSCs on infarcted heart. (**B**) SEM image of MN. Scale bar, 500 μm. (**C**) Representative fluorescent image indicating that DiO-labeled CSCs (green) were encapsulated in fibrin gel and then integrated onto the top surface of MN array (red). Scale bar, 500 μm.

into a microfluidic channel with Iscove's modified Dulbecco's medium (IMDM) (Fig. 2A). LIVE/DEAD staining revealed excellent viability of CSCs on day 3 in culture, and quantitative analysis indicated that the viability of CSCs in fibrin gel was not compromised when cocultured on MN array on days 1, 3, and 7 (Fig. 2B). After 3 days of culture, confocal microscopy was used to assess the distribution of the CSCs (green) within the MN (red) patch (Fig. 2C). *Z*-stack reconstruction showed that some CSCs migrated from the fibrin gel into the MN cavity (Fig. 2C). Since most of the beneficial effects of CSC therapy were through their secretion, we used enzyme-linked immunosorbent assay (ELISA) to measure the concentrations of various CSC-secreted factors, namely, hepatocyte growth factor (HGF), vascular endothelial growth factor (VEGF), and insulin-like growth factor 1 (IGF-1) in the media underneath. The factors could be detected, and their release profiles were similar to those of CSCs cultured on the tissue culture plate (TCP) at various time points (Fig. 2D). We then tested the biocompatibility of the MN-CSC patch in vitro with isolated neonatal rat cardiomyocytes (NRCMs). NRCMs were cultured with the presence of a MN or MN-CSC patch in the media. A solitary NRCM culture was included as a control. LIVE/DEAD assay indicated the viability of NRCMs (Fig. 2E and fig. S2), and quantitative analysis indicated that the morphology and viability of NRCMs were not compromised when cocultured with a MN or MN-CSC patch (Fig. 2, F and G). Moreover, time-lapse videos revealed that coculture with a MN-CSC patch substantially increased cardiomyocyte contractility (Fig. 2H and movies S1 to S3). In addition, MN-CSCs robustly promoted cardiomyocyte proliferation (Fig. 2, I and J). Collectively, these data suggested that the MN patch was nontoxic to cardiomyocytes and that MN-CSCs could promote cardiomyocyte functions.

MN-CSC therapy in a rat MI model

We then went ahead to test the MN-CSC patch in rats with acute MI (Fig. 3A). Immediately after left anterior descending (LAD) artery ligation, a 0.5-cm by 0.5-cm MN-CSC patch containing 1×10^6 rat CSCs was placed onto the MI area (Fig. 3B and movie S4). Hematoxylin and eosin (H&E) staining indicated that the MN-CSC patch was on the surface of infarcted heart on day 7 (Fig. 3C). Cy5.5-labeled MNs could be readily detected on the heart 7 days after the transplantation (Fig. 3D). Furthermore, the tissue densities of $CD68^+$ macrophages were identical across all three groups (Fig. 3E), suggesting that the MN-CSC patch did not aggravate the inflammation in the post-MI heart. In addition, no evident raises in $CD3/CD8^+$ T cell infiltration were observed in the hearts treated with MN-CSC on day 7 (fig. S3). Treatment with the MN-CSC patch reduced myocardial apoptosis (Fig. 3F) and promoted myocyte proliferation (Fig. 3G) and angiogenesis (Fig. 3H). Masson's trichrome staining revealed heart morphology and fibrosis 3 weeks after various treatments (Fig. 4A; red, viable tissue; blue, scar). M-mode echocardiographic images showed the left ventricular (LV) wall motion after different treatments (Fig. 4B). MN-CSC transplantation increased infarct wall thickness (Fig. 4C) and viable tissue in the affected area (Fig. 4D). As a cardiac function indicator, LV ejection fractions (LVEFs) were determined by echocardiography at baseline (4 hours after MI) and 3 weeks afterward. The LVEFs at baseline were indistinguishable among all three groups, indicating a uniform degree

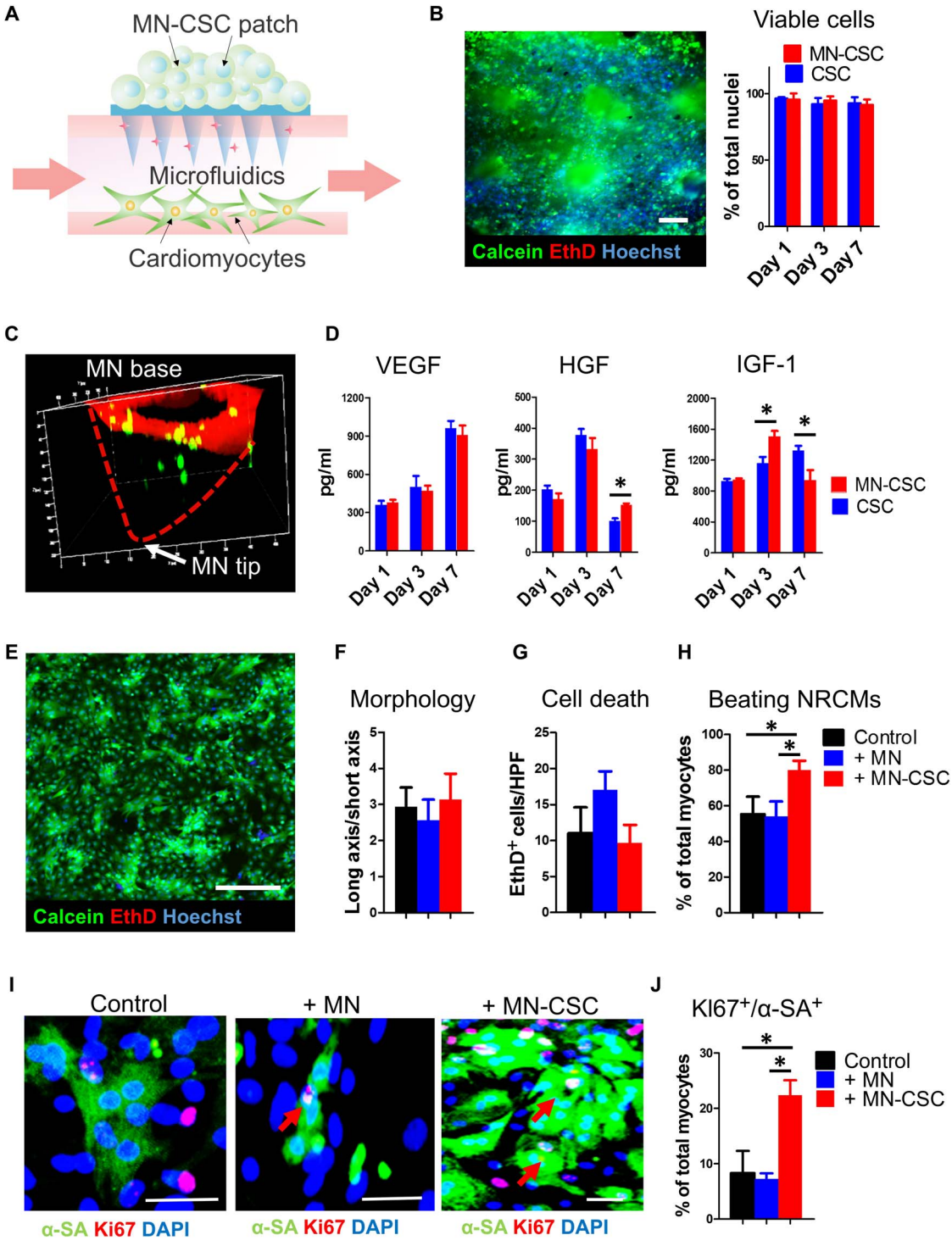

Fig. 2. Effects of MN-CSCs on NRCMs function in vitro. (**A**) Schematic showing the study design used to test the effects of MN-CSCs on NRCMs in vitro. (**B**) Calcein (live)/EthD (dead) staining revealed the viability and morphology of CSCs cultured on the MN patch and the quantitative analysis of CSC viability on days 1, 3, and 7. $n = 3$ for each group at each time points. Scale bar, 200 μm. (**C**) Confocal image indicating CSCs (green) migration from the fibrin gel into the MN cavity after 3 days in culture. (**D**) Releases of various CSC factors (namely VEGF, IGF-1, and HGF). $n = 6$ for each group at each time point. (**E**) Calcein (live)/EthD (dead) staining revealed the morphology and viability of NRCMs 3 days in culture with MN-CSC patch. Scale bar, 200 μm. (**F**) Quantitative analysis of NRCM morphology cultured alone or cocultured with MN or MN-CSC patch at day 3. $n = 6$ for each group. (**G**) Quantitative analysis of cell viability for NRCMs cultured alone or cocultured with MN or MN-CSC patch at day 3. $n = 3$ for each group. HPF, high power field. (**H**) Time-lapse videos revealed coculture with MN-CSC patch significantly increased cardiomyocyte contractility at day 3. $n = 6$ for each group. (**I** and **J**) Representative fluorescent micrographs and quantitative analysis of NRCMs stained with proliferation marker Ki67 (red) and α-sarcomeric actin (α-SA) (green). NRCMs were cultured alone or with MN or MN-CSC patch. $n = 3$ for each group. Scale bars, 50 μm. All data are presented as means ± SD. A two-tailed, unpaired Student's t test was used to compare between any two groups. One-way analysis of variance (ANOVA), followed by post hoc Bonferroni test, was used to compare between three or more groups. *$P < 0.05$. DAPI, 4′,6-diamidino-2-phenylindole.

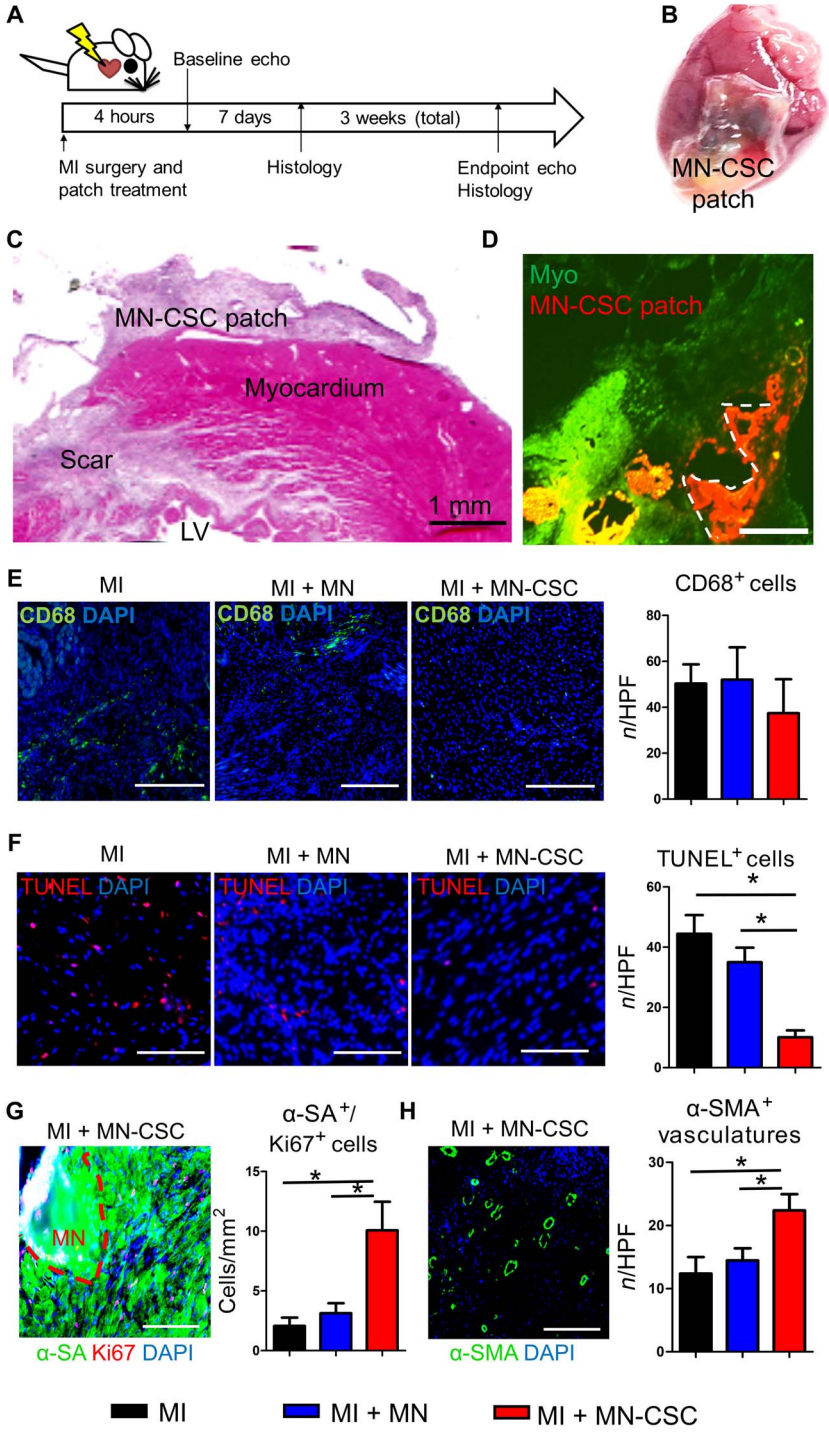

Fig. 3. MN-CSC patch reduces apoptosis and promotes angiomyogenesis in the post-MI heart. (**A**) Schematic showing the overall animal study design used to test the therapeutic benefits of MN-CSCs in a rat model of MI. (**B**) Placement of a MN-CSC patch on the rat heart. (**C**) H&E staining indicating the presence of MN-CSC patch on the infarcted heart. Scale bar, 1 mm. (**D**) Fluorescent image showing Cy5.5-labeled MNs (red) could be readily detected on the heart (green) 7 days after the transplantation. Scale bar, 400 μm. (**E**) Representative fluorescent micrographs showing the presence of $CD68^+$ cells (green) in the control MI heart or hearts treated with MN or MN-CSC patch at day 7. The numbers of $CD68^+$ cells were quantified. $n = 3$ hearts for each group. Scale bar, 200 μm. (**F**) Representative fluorescent micrographs showing the presence of $TUNEL^+$ (terminal deoxynucleotidyl transferase–mediated deoxyuridine triphosphate nick end labeling–positive) apoptotic cells (red) in the MI hearts treated alone or treated with MN or MN-CSC patch at day 7. The numbers of $TUNEL^+$ apoptotic cells were quantified. $n = 3$ for each group. Scale bars, 100 μm. (**G**) Representative fluorescent micrograph showing the presence of $Ki67^+$ cardiomyocyte nuclei (red) in the MI hearts treated with MN-CSC on day 7. The numbers of $Ki67^+$ nuclei were quantified in MI-, MI + MN-, or MI + MN-CSC–treated hearts. $n = 3$ for each group. Scale bar, 200 μm. (**H**) Representative fluorescent micrograph showing the presence of α–smooth muscle actin (α-SMA; green) in the MI hearts treated with MN-CSC on day 7. The numbers of α-SMA^+ vasculatures were quantified in MI-, MI + MN-, or MI + MN-CSC–treated hearts. $n = 3$ for each group. Scale bar, 200 μm. All data are presented as means ± SD. Comparisons between three or more groups were performed using one-way ANOVA, followed by post hoc Bonferroni test. *$P < 0.05$.

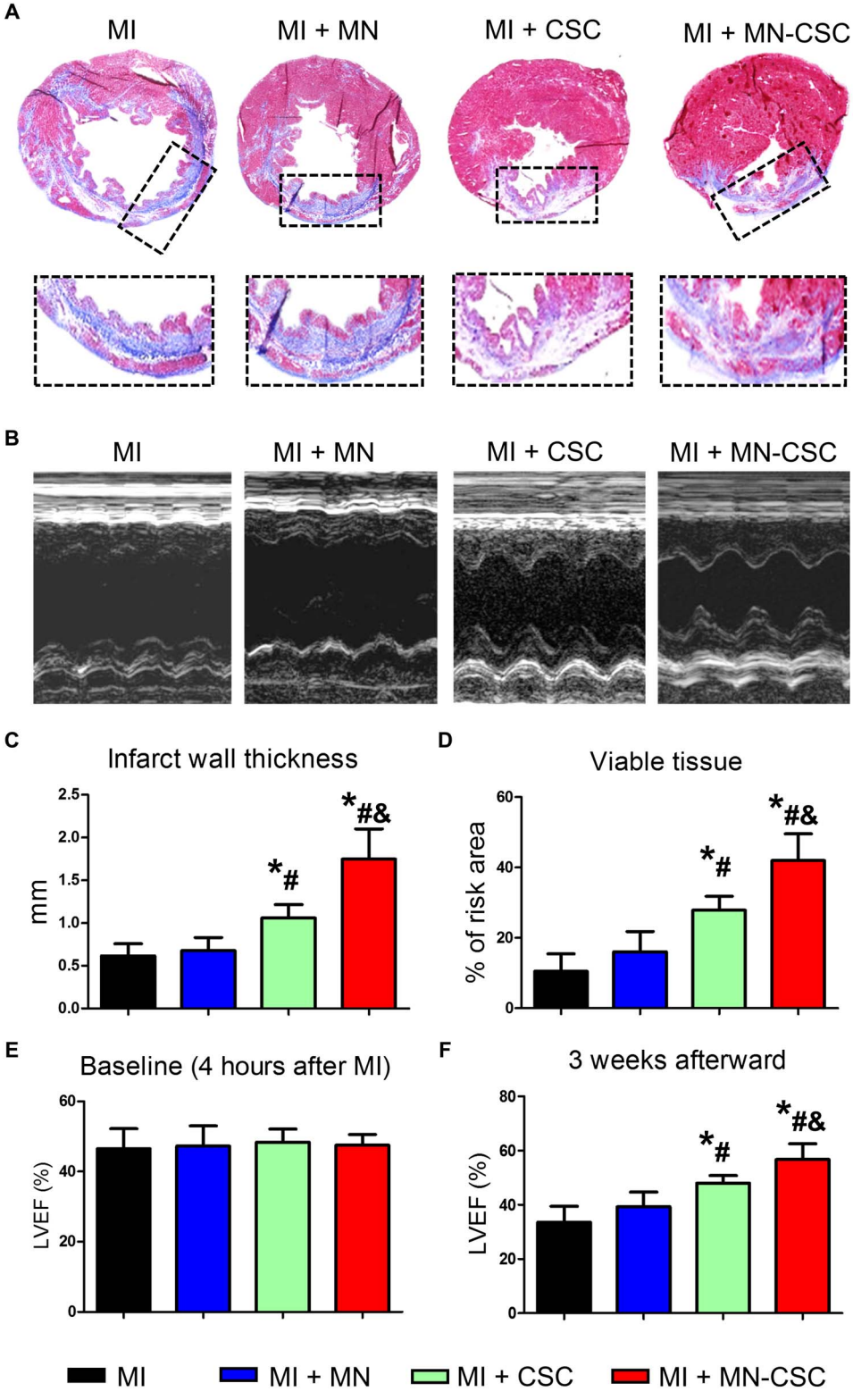

Fig. 4. MN-CSC ameliorates ventricular dysfunction and promotes cardiac repair in a rat model of heart attack. (**A**) Representative Masson's trichrome–stained myocardial sections 3 weeks after MI. Blue, scar tissue; red, viable myocardium; snapshots, high-magnification images of the black box area. (**B**) Representative M-mode echocardiographic images showing the LV wall motion of the hearts. (**C** and **D**) Quantitative analyses of (C) infarct wall thickness and (D) viable tissue in the risk area based on Masson's trichrome staining. $n = 6$ animals per group. (**E** and **F**) LVEFs measured by echocardiography at 4 hours (baseline) and 3 weeks (endpoint) after MI. $n = 6$ animals per group. All data are presented as means ± SD. Comparisons between three or more groups were performed using one-way ANOVA, followed by post hoc Bonferroni test. $^{*}P < 0.05$ when compared with the MI group; $^{\#}P < 0.05$ when compared with the MI + MN group; $^{\&}P < 0.05$ when compared with the MI + CSC group.

of initial injury (Fig. 4E). Three weeks after treatment, the hearts that received MN-CSC transplantation had the greatest LVEFs (Fig. 4F). Compared to the MI control animals, the empty MN patch generated neither beneficial nor detrimental effects in the post-MI heart. Additional rat studies were performed to compare the treatment effects from a PVA patch with CSCs but no MNs (No–MN-CSC group) and a MN CSC patch (MN-CSC). Masson's trichrome staining revealed heart morphology and fibrosis 3 weeks after treatment (fig. S4A; red, viable tissue; blue, scar tissue). Compared to the non-MN control, infarcted sizes were effectively controlled by MN-CSC patch transplantation (fig. S4B). Also, viable tissue in the risk area (fig. S4C) and infarct wall thickness (fig. S4D) were greater with MN-CSC patch treatment. The LVEFs at baseline were indistinguishable between these two groups, indicating a similar degree of initial injury (fig. S5A). Three weeks after, the hearts that received MN-CSC patches had greater LVEFs (fig. S5B). To address the toxicity issue of PVA patches, we measured serum alanine aminotransferase (ALT), aspartate transaminase (AST) (for liver functions) (fig. S6, A and B), and creatinine and blood urea nitrogen (BUN) levels (for kidney functions) (fig. S6, C and D) 21 days after patch transplantation. The results indicate that patch treatment did not induce any hepatic or renal function impairment. Together, these results indicate that the MNs on the MN-CSC patches are indispensable for the full therapeutic benefit. We reason that the MNs provide a pathway for molecules to diffuse from the CSCs to the site of injury (Figs. 2C and 3D) more efficiently than the non-MN controls.

MN-CSC therapy in a porcine model of acute MI

Despite the widespread use of rodent models for cellular cardiomyopathy, the use of the porcine model is well justified, as the pig heart has human-like myocardial blood flow, ventricular mechanics, and dimensions. Therefore, we performed a pilot porcine study on MN-CSC cardiac patch. The safety and preliminary therapeutic efficacy were determined in pigs with acute MI induced by LAD permanent ligation (Fig. 5A). Successful open-chest surgical induction of MI was verified by the elevation of the ST segment on electrocardiogram (ECG) and cardiac troponin I (cTnI) level in serum (Fig. 5B and fig. S7). Triphenyl tetrazolium chloride (TTC) staining of porcine heart sections determined the infarct area 48 hours after MI (Fig. 5D). The infarct sizes were the same across the two groups (Fig. 5C). The baseline (4 hours after MI) and endpoint (48 hours after infarct) LVEFs were measured as indicators of cardiac functions in both groups. The baseline LVEFs were similar for both control and MN-CSC patch groups, which indicated a similar degree of initial injury (Fig. 6A). However, MN-CSC–treated group exhibited greater LVEFs than those from the control group at 48 hours (Fig. 6B). LV fractional shortening (LVFS) showed a similar trend (Fig. 6, D and E). We also calculated treatment effects, i.e., the changes in LVEF and LVFS from the baseline to the endpoint. While the control group displayed a functional decline, treatment with MN-CSC patches preserved cardiac functions (Fig. 6, C and F). To address the toxicity concerns of the MN-CSC patch, blood was collected and tested at baseline (before MI surgery) and 48 hours after MI. The concentrations of ALT and AST indicated that liver functions were not impaired by the MN-CSC therapy (Fig. 6, G and H). Also, the creatinine and BUN analyses indicated that MN-CSC patch treatment did not induce any renal function impairment (Fig. 6, I and J). Together, we conclude that MN-CSC patch transplantation after acute MI could contribute to the preservation of cardiac function without inducing toxicity.

DISCUSSION

"A bandage for a broken heart" has always been a dream for cardiologists and tissue engineers. Here, we integrated therapeutic CSCs with a MN array to form an innovative "cardiac patch." Unlike conventional cardiac patches (*31*–*33*), the prickly MNs can serve as the communication channels between the transplanted CSCs and the host myocardium. PVA has been widely used to fabricate hydrogels for medical application because of its excellent biocompatibility (*34*–*36*). In addition, PVA is used for MN fabrication here because of its high mechanical strength in dry state and its ability to transport solute in gel state after being inserted to skins, where PVA MN could maintain its integrity as a gel within a short term (*35*, *37*, *38*), and eventually get dissolved and absorbed by skins over a long period (*39*, *40*). Thus, the slow dissolution rate of PVA also provides sustained release of regenerative factors from the encapsulated CSCs. While biodegradable polymers are advantageous for medical applications, the degradation by-products and fragmentation of these polymers may cause side effects as well. Providing the proof of concept in the present studies, future studies will focus on the optimization of biodegradability and biocompatibility of the polymers for the MN-CSC patches.

The in vitro experiment emulated the placement of the MN-CSC patch on the surface of a heart to answer two questions: (i) Can the media support CSC growth in the integrated device? and (ii) Can CSC-derived factors be released into the media underneath? (Fig. 2). We found that the viability of CSCs cultured on the MN patch was not compromised, indicating that neither the PVA nor the fibrin gel was toxic to the cells. Furthermore, CSC-secreted factors were able to diffuse through the needles into the media. We then cultured cardiomyocytes (NRCMs) in the media underneath the MN-CSC patch. The viability of cardiomyocytes was not affected by the placement of the MN-CSC patch. Instead, coculturing with the MN-CSC patch promoted cardiomyocyte proliferation and beating. This was consistent with the observation when cardiomyocytes were cocultured with CSCs (*41*, *42*).

We then evaluated the in vivo biocompatibility of the MN-CSC patch in rats with acute MI. Syngeneic rat CSCs were used to avoid rejection of the transplanted cells. Nevertheless, foreign body reactions could be triggered against the materials and structures of the MN patch. It was confirmed that the MN-CSC could be successfully placed onto the surface of the heart without the deconstruction of the needles (Fig. 3). Moreover, the insertion of MNs (400 to 500 μm) caused negligible cardiac tissue damage (Fig. 3). The myocardial tissue density of $CD68^+$ macrophages was indistinguishable among the groups (Fig. 3), and there is no evidence of elevated infiltrations of CD3/CD8-positive T cells in the heart treated with the MN-CSC patch (fig. S3). In addition, the normal levels of ALT, AST, BUN, and creatinine in the pig model treated with a MN patch confirmed the safety and biocompatibility of the cardiac patch (Fig. 6). This was consistent with the notion that PVA is a material with great biocompatibility.

Next, we tested the hypothesis that the transplanted MN-CSC patch could serve as a mini-drug plant for sustained release of regenerative factors. Previous reports indicated that transplantation of CSCs stimulated endogenous repair by reducing apoptosis and promoting angiomyogenesis (*12*, *42*). However, these effects were not long lasting because of the poor retention/engraftment of CSCs. These caveats were overcome by the MN-CSC strategy. MN-CSC therapy robustly reduced myocardial apoptosis but increased the numbers

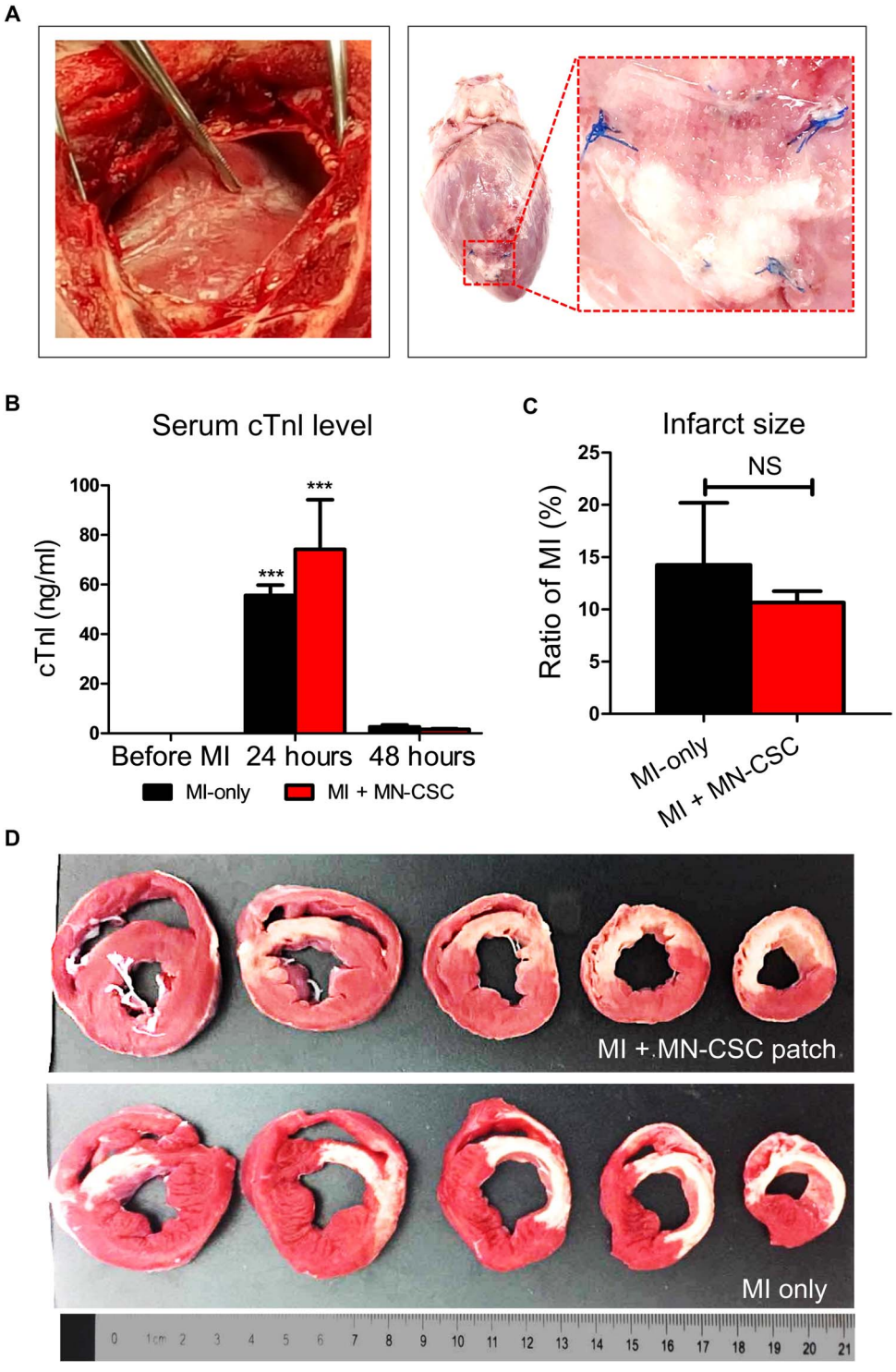

Fig. 5. Induction of MI in the swine by LAD ligation. (**A**) Representative images of LAD ligation (left) and MN-CSC patch placement on the heart (right). (**B**) Serum concentration of cTnI before MI and 24 hours/48 hours after MI. All data are presented as means ± SD. $n = 3$ animals per group. ***$P < 0.001$ when compared with baseline (before MI) and 48 hours after MI. Black bar, MI-only group; red bar, MN-CSC patch–transplanted group. (**C**) Quantitative analyses of infarct size at 48 hours after MI through calculation. All data are presented as means ± SD. $n = 3$ animals per group. NS (not significant) indicates $P > 0.05$ when compared between two groups. Black bar, MI-only group; red bar, MN-CSC patch–transplanted group. (**D**) Macroscopic TTC staining images representing infarct area on multiple slices of an infarcted pig heart.

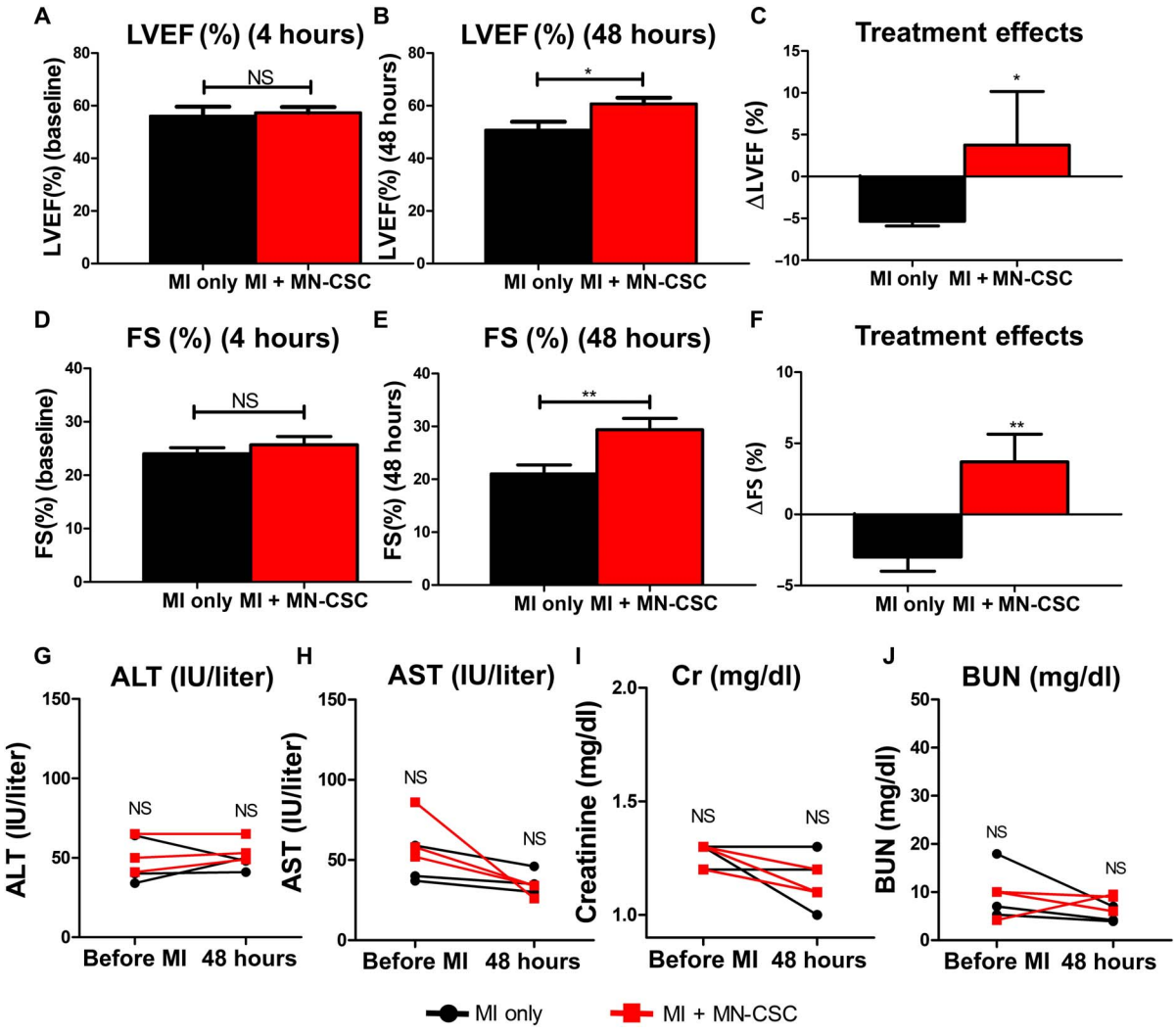

Fig. 6. MN-CSC therapy ameliorates ventricular dysfunction and promotes cardiac repair in a swine model of MI. (**A** to **C**) LVEFs determined by echocardiography at baseline (A) (4 hours after infarct) and endpoint (B) (48 hours after infarct). The treatment effects are calculated as the change of LVEFs from endpoint to baseline (C). (**D** to **F**) Fractional shortenings (FSs) determined by echocardiography at baseline (D) (4 hours after infarct) and endpoint (E) (48 hours after infarct). The treatment effects are calculated as the change of FSs from baseline to endpoint (F). All data are presented as means ± SD. $n = 3$ animals per group. $^{**}P < 0.01$ when compared between two groups. Black bars, MI-only group; red bars, MN-CSC patch–transplanted group. (**G** to **J**) ALT (G), AST (H), creatinine (I), and BUN (J) are evaluated at baseline (before MI) and endpoint (48 hours after MI). Black, MI-only group; red, MN-CSC patch–transplanted group. All data are presented as means ± SD. $n = 3$ animals per group. NS indicates $P > 0.05$.

of cycling cardiomyocytes and vasculatures in the peri-infarct area. Furthermore, these protective and regenerative effects at the cellular level translated into the improvement of overall heart morphology and pump function (Fig. 4). The hearts that received the MN-CSC patch had the greatest wall thicknesses, viable tissues, and LVEFs. Following an acute MI, the heart could undergo severe remodeling, which includes the thinning of LV wall, the replacement of healthy myocardium with scar, and the continuous deterioration of cardiac function. Transplantation of a MN-CSC patch was not only able to alter this trajectory of maladaptive remolding but also promoted cardiac repair. Moreover, the safety and efficacy of MN-CSC cardiac patch were evaluated in a pig model of acute MI. The result supported the notion that MN-CSC patch transplantation could preserve cardiac pump function (Fig. 6).

It is worth noting that we delivered the MN-CSC patch through open-chest surgery. In the future, minimally invasive approaches should be explored to deploy this patch on the surface of the heart. Further studies could also focus on the design of "smart" MN patches that release regenerative factors in response to physiological environmental stimulus in the post-MI heart (*43*, *44*).

MATERIALS AND METHODS

Derivation of rat CSCs

This methodology was taken from our previous study (*45*). CSCs were explanted from Wistar-Kyoto (WKY) rat hearts. Myocardial samples were excised from WKY rats and cut into 2-mm^3 fragments. These were washed with PBS and partially digested with collagenase (Sigma-Aldrich). They were then cultured in IMDM (Invitrogen, Carlsbad, CA, USA) containing 20% fetal bovine serum (FBS) (Corning, Corning, NY, USA) as cardiac explants on a fibronectin (Corning)–coated surface

(0.5 mg/ml). Stromal-like cells and phase-bright cells emerged from the cardiac explant. The explant-derived cells were passaged with TrypLE Select (Gibco). Passaged cells were seeded in Ultra-Low attachment flasks (Corning, Corning, NY) at a density of 2×10^4 cells/ml. The spontaneous aggregation of these explant-derived cells into cardiospheres was observed after 1 week. The cardiospheres were then passaged into fibronectin-coated surfaces to complete the generation of cardiosphere-derived CSCs. All cultures were incubated in 5% CO_2 at 37°C.

Fabrication and characterization of MNs

This methodology was taken from our previous study (*46*). MNs were fabricated using five uniform silicone molds from Blueacre Technology Ltd. The MNs have a 300-μm-diameter round base, which tapers for a height of 600 μm before ending in a tip that is roughly 5 μm in radius. The MNs were arranged 600 μm apart, tip to tip, in a 20 by 20 array. First, aqueous PVA solution (10 weight %, 100 μl) was prepared and deposited in a silicone mold, which was kept under vacuum for 20 min. The mold was then centrifuged at 500 rpm for 20 min in a Hettich Universal 32R centrifuge to compact the gel solution into MN cavities. Then, additional aqueous solutions of PVA (100 μl) were loaded into the mold, and the above procedure was repeated several times, until a total volume of 500 μl of PVA solution was added to the mold. Last, each micromold was dried under vacuum for another 24 hours. Once dried, the MN array patch was carefully separated from the silicone mold for further application. An FEI Verios 460L field-emission scanning electron microscope was used to assess the morphology of the MNs. Cy5.5-labeled PVA MN was prepared similarly. In short, Cy5.5 was first used to modify PEG_{5K}-NH_2, which was subsequently dissolved in PVA aqueous solution to label the MN. The modification of Cy5.5 with PEG_{5K} could increase its water solubility and retention in MN. A stress-strain gauge was used to determine the mechanical strength of the MNs by pressing a stainless steel plate toward the MNs on a DTS delaminator. The initial gauge between the tips of MN and the plate was 2.00 mm, with the load cell capacity of 10.00 N. The plate approached MNs at a speed of 0.1 mm/s. The force that led to the failure of MNs was defined as the force at which the needle began to buckle.

Preparation of MN-CSCs

This methodology was taken from our previous study (*12*). CSCs were first encapsulated in fibrin gel (Baxter Healthcare Corp.) and then placed on the basal side of MN patch to form MN-CSC. In vitro, the MN-CSC patch was cultured in a four-well chamber with 20% FBS media. The viability of the cells was evaluated with a LIVE/DEAD Viability/Cytotoxicity kit on days 1, 3, and 7. For confocal imaging, DiO-labeled CSCs were encapsulated in fibrin gel and placed on the basal side of a Cy5.5-labeled MN patch. After 3 days of culture, the MN patch was imaged using a confocal microscope (Zeiss LSM 880).

In vitro cytokine release

This methodology was taken from our previous study (*47*). Rat CSCs (1×10^5) or MN-CSC containing 1×10^5 rat CSCs were cultured in 1 ml of FBS-free media in a 24-well plate. Conditioned media were collected from the plates on days 1, 3, and 7 to study the cells' release of growth factors. The concentrations of various growth factors in the media were measured by ELISA kits (R&D Systems, Minneapolis, MN; B-Bridge International, Cupertino, CA) as per the manufacturer's instructions. The growth factors assayed were HGF, VEGF, and IGF-1.

Culture of NRCMs with MN-CSCs

NRCMs were derived from Sprague-Dawley rats as previous described (*48*). We cultured NRCMs in a four-well chamber. A MN or MN-CSC patch was placed on the surface of NRCMs. A solitary NRCM culture was included as a control. A LIVE/DEAD Viability/Cytotoxicity kit was used to determine the cell viability of NRCMs at day 3. The morphology of the cells was characterized using National Institutes of Health (NIH) ImageJ software. Cell proliferation was evaluated by the percentage of α-SA/Ki67-positive cardiomyocytes by immunocytochemistry staining.

Immunogenicity studies on MN-CSC

Rats were anesthetized with ketamine. Then, their hearts were exposed by left thoracotomy under sterile conditions. An MN-CSC patch containing 1×10^6 CSCs was placed onto the heart. Those rats that underwent the left thoracotomy but did not receive a patch were set as normal control. After 7 days, all rats were sacrificed, and hearts were collected and cryopreserved in optimum cutting temperature (OCT) compound. They were then cryosectioned and fixed with 4% paraformaldehyde. Protein block solution (Dako, Carpinteria, CA) containing 0.1% saponin (Sigma-Aldrich, St. Louis, MO) was used to permeabilize and protein-block each section. The following primary antibodies were used to target the desired proteins after an overnight incubation at 4°C: mouse anti-CD8α (1:100; MCA48R, AbD Serotec, Raleigh, NC) and rabbit anti-CD3 (1:100; ab16669, Abcam). Subsequently, fluorescein isothiocyanate (FITC) secondary antibodies (1:100; Abcam) were used for the detection of primary antibodies. DAPI (Life Technologies, NY, USA) was used to counterstain cell nuclei. Images were taken with an Olympus epifluorescence microscope.

Rat model of MI

All animal work was compliant with the Institutional Animal Care and Use Committee at North Carolina State University. This methodology was taken from our previous study (*49*). Briefly, rats were anesthetized with ketamine and were positioned right laterally on a sterile operating table. Their hearts were exposed by left thoracotomy, and their LAD coronary arteries were permanently ligated to produce an acute MI. Immediately after MI induction, one of the following randomized treatments was administered to each rat: (i) MI group: MI induction without any treatment; (ii) MI + MN group: MN patch was placed onto the surface of infarcted heart; (iii) MI + CSC group: CSCs (1×10^6) encapsulated in fibrin gel were placed onto the infarcted heart; (iv) MI + MN-CSC group: MN-CSCs patch containing 1×10^6 CSCs was placed onto the infarcted heart. After patch application with a gentle pressure by tweezer tips for 30 s, we applied fibrin glue on the MN side of the patch to aid adhesion.

Transplantation of patches with or without MNs in rats with MI

All animal work was compliant with the Institutional Animal Care and Use Committee at North Carolina State University. Briefly, rats were anesthetized with ketamine. Immediately after MI induction (*49*), animals were randomized to receive one of the following two treatments: (i) MI + No–MN-CSC group: a PVA patch without MNs containing 1×10^6 CSCs was placed onto the infarcted heart; (ii) MI + MN-CSC group: a MN-CSC patch containing 1×10^6 CSCs was placed onto the infarcted heart. Serum ALT, AST, creatinine, and

BUN levels were measured 21 days after transplantation. Normal range for rats is as follows: ALT, 10 to 40 IU/liter; AST, 50 to 150 IU/liter (*50*); creatinine, 0.1 to 0.55 mg/dl; BUN, 3.56 to 25.43 mg/dl (*51*).

Pig model of MI

All animal work was compliant with the Institutional Animal Care and Use Committee at North Carolina State University. Acute MI was induced in female Yorkshire pigs (20 to 30 kg) by permanent ligation of LAD during an open-chest surgery (*52*). Twenty minutes after ischemia, a 2.5-cm by 2.5-cm MN-CSC cardiac patch was placed on the heart to cover the MI-injured area that is downstream of LAD (Silkam 2/0, B. Braun Suture). The control animals received no cardiac patches. After the procedures, all animals were closely monitored by university veterinary services staff, and then the pigs were euthanized 48 hours after MI injury. LVEFs were determined by echocardiography using a Philips CX30 ultrasound system, coupled with an S4-2 high-frequency probe at two time points (4 and 48 hours after MI). Blood was collected before MI and 24 and 48 hours after MI. Infarct area of LV myocardium was traced through the digital images of TTC staining (five slices) and measured by ImageJ analysis. Then, the infarct ratio was measured and calculated as Infarct size $= \frac{\sum_{n=1}^{5}(\text{slice infarcted area}\% \times \text{slice weight})}{\text{heart weight}} \times 100\%$.

TTC assay

This methodology was taken from our previous study (*45*). TTC assay was performed to differentiate the active cardiac tissue and the inactive infarct cardiac tissue. A sterilized solution of TTC was made by dissolving TTC (2 g; MP Biomedicals LLC) into 200 ml of sterilized PBS and then prewarmed at 37°C in the incubator for 30 min. The heart was collected and washed with sterilized PBS and then placed in a freezer until the heart became stiff. Five 7-mm sections were cut from apex to bottom and incubated in prewarmed TTC solution at 37°C for 30 min. Afterward, 10% formaldehyde solution was applied for 2 hours to fix the sections.

Cardiac function assessment

This methodology was taken from our previous study (*12*). Rats were anesthetized with isoflurane/oxygen mixture before undergoing transthoracic echocardiography in the supine position at 4 hours and 3 weeks. An animal cardiologist who was blinded to the experimental design performed the procedure using a Philips CX30 ultrasound system with a L15 high-frequency probe. The hearts were viewed in two-dimension (2D) along the long axis, at the height of the greatest LV diameter. The following formula was used to determine the EF: (LVEDV − LVESV/LVEDV) ×100%. 2D guided ultrasound images were captured in motion mode at the level of the chordae tendineae.

Heart morphometry

This methodology was taken from our previous study (*12*). All animals were sacrificed 3 weeks after MI induction, after the echocardiography study. Hearts were collected and cryopreserved in OCT compound. Heart sections (10 μm thick) were cut from the apex to the height of the ligation. Each section was cut at 100-μm intervals. Masson's trichrome [HT15 Trichrome Staining (Masson) Kit, Sigma-Aldrich] staining was performed according to the manufacturer's specifications. A PathScan Enabler IV slide scanner (Advanced Imaging Concepts, Princeton, NJ) was used to acquire images of each stained section. These were used to assess morphometric parameters (i.e., infarct thickness and viable myocardium), which were quantified with NIH ImageJ software.

Histology

This methodology was taken from our previous study (*12*). For immunohistochemistry, heart cryosections were fixed with 4% paraformaldehyde. Permeabilization and protein blocking were done with protein block solution (Dako, Carpinteria, CA) containing 0.1% saponin (Sigma-Aldrich, St. Louis, MO). Proteins of interest in the samples were targeted with the following primary antibodies after an overnight incubation at 4°C: rabbit anti-Ki67 (1:100; ab15580, Abcam), mouse anti-CD68 (1:100; ab955, Abcam), mouse anti–α-SA (1:100; a7811, Sigma-Aldrich), and mouse anti-actin α–smooth muscle (1:100; A5228, Sigma-Aldrich). Primary antibodies were conjugated with FITC or Texas Red secondary antibodies (1:100; Abcam). For the cell apoptosis assays, heart cryosections were incubated with TUNEL solution (Roche Diagnostics GmbH, Mannheim, Germany). DAPI (Life Technologies, NY, USA) was used for nuclear staining. Images were taken with an Olympus epifluorescence microscope.

For H&E staining, sections were fixed in hematoxylin (Sigma-Aldrich, MO, USA) for 5 min at room temperature and then rinsed for 2 min in running water. The sections were then dipped in acid alcohol for 2 s, in sodium bicarbonate (five dips), and in dehydrant (Richard-Allan Scientific, MI, USA) for 30 s. They were subsequently submerged in eosin (Sigma-Aldrich, MO, USA) for 2 min and thoroughly washed in dehydrant and xylene (VWR, PA, USA).

Statistical analysis

This methodology was taken from our previous study (*12*). Results are shown as means ± standard deviation. A two-tailed Student's *t* test was used to compare between two groups. One-way ANOVA, followed by post hoc Bonferroni test, was used to compare among three or more groups. If the *P* value is <0.05, the difference in means is considered statistically significant.

SUPPLEMENTARY MATERIALS

Supplementary material for this article is available at http://advances.sciencemag.org/cgi/content/full/4/11/eaat9365/DC1

Fig. S1. Characterization of PVA MN.
Fig. S2. Characterization of NRCMs cultured with MN.
Fig. S3. Local T cell immune response in immunocompetent rat treated with a MN-CSC patch.
Fig. S4. MN-CSC therapy protects cardiac morphology and reduces fibrosis in a rat model of MI.
Fig. S5. Cardiac functions at baseline and 3 weeks after MI + No–MN-CSC or MI + MN-CSC treatment.
Fig. S6. Effects of PVA patches on kidney and liver functions 21 days after transplantation.
Fig. S7. Changes in ECG parameters from pre-LAD ligation to post-LAD ligation in swine study.
Movie S1. Beating NRCMs cultured alone on TCP.
Movie S2. Beating NRCMs cultured with a MN patch on TCP.
Movie S3. Beating NRCMs cultured with a MN patch loaded with CSCs (MN-CSCs) on TCP.
Movie S4. MN patch loaded with CSCs (MN-CSCs) placed on the surface of an infarcted rat heart.

REFERENCES AND NOTES

1. E. J. Benjamin, M. J. Blaha, S. E. Chiuve, M. Cushman, S. R. Das, R. Deo, S. D. De Ferranti, J. Floyd, M. Fornage, C. Gillespie, C. R. Isasi, M. C. Jim'nez, L. C. Jordan, S. E. Judd, D. Lackland, J. H. Lichtman, L. Lisabeth, S. Liu, C. T. Longenecker, R. H. MacKey, K. Matsushita, D. Mozaffarian, M. E. Mussolino, K. Nasir, R. W. Neumar, L. Palaniappan, D. K. Pandey, R. R. Thiagarajan, M. J. Reeves, M. Ritchey, C. J. Rodriguez, G. A. Roth, W. D. Rosamond, C. Sasson, A. Towfghi, C. W. Tsao, M. B. Turner, S. S. Virani, J. H. Voeks, J. Z. Willey, J. T. Wilkins, J. H. Y. Wu, H. M. Alger, S. S. Wong, P. Muntner, Heart disease and stroke statistics'2017 update: A report from the american heart association. *Circulation* **135**, e146–e603 (2017).
2. P. S. Jhund, J. J. V. McMurray, Heart failure after acute myocardial infarction: A lost battle in the war on heart failure? *Circulation* **118**, 2019–2021 (2008).
3. E. Marbán, Breakthroughs in cell therapy for heart disease: Focus on cardiosphere-derived cells. *Mayo Clin. Proc.* **89**, 850–858 (2014).

4. R. Madonna, P. Ferdinandy, R. De Caterina, J. T. Willerson, A. J. Marian, Recent developments in cardiovascular stem cells. *Circ. Res.* **115**, e71–e78 (2014).
5. A. J. Boyle, S. P. Schulman, J. M. Hare, Stem cell therapy for cardiac repair: Ready for the next step. *Circulation* **114**, 339–352 (2006).
6. V. F. M. Segers, R. T. Lee, Stem-cell therapy for cardiac disease. *Nature* **451**, 937–942 (2008).
7. O. Lindvall, Z. Kokaia, Stem cells for the treatment of neurological disorders. *Nature* **441**, 1094–1096 (2006).
8. I. J. Fox, G. Q. Daley, S. A. Goldman, J. Huard, T. J. Kamp, M. Trucco, Use of differentiated pluripotent stem cells in replacement therapy for treating disease. *Science* **345**, 1247391 (2014).
9. C. P. Hodgkinson, A. Bareja, J. A. Gomez, V. J. Dzau, Emerging concepts in paracrine mechanisms in regenerative cardiovascular medicine and biology. *Circ. Res.* **118**, 95–107 (2016).
10. J. Walter, L. B. Ware, M. A. Matthay, Mesenchymal stem cells: Mechanisms of potential therapeutic benefit in ARDS and sepsis. *Lancet Respir. Med.* **2**, 1016–1026 (2014).
11. Z. Lin, W. T. Pu, Strategies for cardiac regeneration and repair. *Sci. Transl. Med.* **6**, 239rv1 (2014).
12. J. Tang, D. Shen, T. G. Caranasos, Z. Wang, A. C. Vandergriff, T. A. Allen, M. T. Hensley, P.-U. Dinh, J. Cores, T.-S. Li, J. Zhang, Q. Kan, K. Cheng, Therapeutic microparticles functionalized with biomimetic cardiac stem cell membranes and secretome. *Nat. Commun.* **8**, 13724 (2017).
13. K. Cheng, D. Shen, M. T. Hensley, R. Middleton, B. Sun, W. Liu, G. De Couto, E. Marbán, Magnetic antibody-linked nanomatchmakers for therapeutic cell targeting. *Nat. Commun.* **5**, 4880 (2014).
14. D. Shen, J. Tang, M. T. Hensley, T. Li, T. G. Caranasos, T. Zhang, Effects of matrix metalloproteinases on the performance of platelet fibrin gel spiked with cardiac stem cells in heart repair. *Stem Cells Transl. Med.* **5**, 793–803 (2016).
15. R. R. Makkar, R. R. Smith, K. Cheng, K. Malliaras, L. E. J. Thomson, D. Berman, L. S. C. Czer, L. Marbán, A. Mendizabal, P. V. Johnston, S. D. Russell, K. H. Schuleri, A. C. Lardo, G. Gerstenblith, E. Marbán, Intracoronary cardiosphere-derived cells for heart regeneration after myocardial infarction (CADUCEUS): A prospective, randomised phase 1 trial. *Lancet* **379**, 895–904 (2012).
16. K. Malliaras, R. R. Makkar, R. R. Smith, K. Cheng, E. Wu, R. O. Bonow, L. Marbán, A. Mendizabal, E. Cingolani, P. V. Johnston, G. Gerstenblith, K. H. Schuleri, A. C. Lardo, E. Marbán, Intracoronary cardiosphere-derived cells after myocardial infarction: Evidence of therapeutic regeneration in the final 1-year results of the CADUCEUS Trial. *J. Am. Coll. Cardiol.* **63**, 110–122 (2014).
17. K. U. Hong, R. Bolli, Cardiac stem cell therapy for cardiac repair. *Curr. Treat. Options Cardiovasc. Med.* **16**, 324 (2014).
18. P. K. Nguyen, E. Neofytou, J.-W. Rhee, J. C. Wu, Potential strategies to address the major clinical hurdles facing stem cell regenerative therapy for cardiovascular disease: A review. *JAMA Cardiol.* **1**, 953–962 (2016).
19. Y. L. Tang, Y. Tang, Y. C. Zhang, K. Qian, L. Shen, M. I. Phillips, Improved graft mesenchymal stem cell survival in ischemic heart with a hypoxia-regulated heme oxygenase-1 vector. *J. Am. Coll. Cardiol.* **46**, 1339–1350 (2005).
20. M. Li, J. C. Izpisua Belmonte, Mending a faltering heart. *Circ. Res.* **118**, 344–351 (2016).
21. R. Madonna, L. W. Van Laake, S. M. Davidson, F. B. Engel, D. J. Hausenloy, S. Lecour, J. Leor, C. Perrino, R. Schulz, K. Ytrehus, U. Landmesser, C. L. Mummery, S. Janssens, J. Willerson, T. Eschenhagen, P. Ferdinandy, J. P. G. Sluijter, Position paper of the European Society of Cardiology Working group Cellular Biology of the Heart: Cell-based therapies for myocardial repair and regeneration in ischemic heart disease and heart failure. *Eur. Heart J.* **37**, 1789–1798 (2016).
22. V. F. M. Segers, R. T. Lee, S. Dimmeler, D. Losordo, Biomaterials to enhance stem cell function in the heart. *Circ. Res.* **109**, 910–922 (2011).
23. J. Yu, Y. Zhang, Y. Ye, R. DiSanto, W. Sun, D. Ranson, F. S. Ligler, J. B. Buse, Z. Gu, Microneedle-array patches loaded with hypoxia-sensitive vesicles provide fast glucose-responsive insulin delivery. *Proc. Natl. Acad. Sci. U.S.A.* **112**, 8260–8265 (2015).
24. M. R. Prausnitz, Microneedles for transdermal drug delivery. *Adv. Drug Deliv. Rev.* **56**, 581–587 (2004).
25. J. Yu, Y. Zhang, W. Sun, A. R. Kahkoska, J. Wang, J. B. Buse, Z. Gu, Insulin-responsive glucagon delivery for prevention of hypoglycemia. *Small* **13**, 1603028 (2017).
26. Y. Ye, J. Wang, Q. Hu, G. M. Hochu, H. Xin, C. Wang, Z. Gu, Synergistic transcutaneous immunotherapy enhances antitumor immune responses through delivery of checkpoint inhibitors. *ACS Nano* **10**, 8956–8963 (2016).
27. J. Yu, Y. Zhang, Z. Gu, Glucose-responsive insulin delivery by microneedle-array patches loaded with hypoxia-sensitive vesicles. *Methods Mol. Biol.* **1570**, 251–259 (2017).
28. C. Chiappini, E. De Rosa, J. O. Martinez, X. Liu, J. Steele, M. M. Stevens, E. Tasciotti, Biodegradable silicon nanoneedles delivering nucleic acids intracellularly induce localized in vivo neovascularization. *Nat. Mater.* **14**, 532–539 (2015).
29. O. Olatunji, D. B. Das, M. J. Garland, L. Belaid, R. F. Donnelly, Influence of array interspacing on the force required for successful microneedle skin penetration: Theoretical and practical approaches. *J. Pharm. Sci.* **102**, 1209–1221 (2013).
30. S. P. Davis, B. J. Landis, Z. H. Adams, M. G. Allen, M. R. Prausnitz, Insertion of microneedles into skin: Measurement and prediction of insertion force and needle fracture force. *J. Biomech.* **37**, 1155–1163 (2004).
31. S. B. Seif-Naraghi, J. M. Singelyn, M. A. Salvatore, K. G. Osborn, J. J. Wang, U. Sampat, O. L. Kwan, G. M. Strachan, J. Wong, P. J. Schup-Magoffin, R. L. Braden, K. Bartels, J. A. DeQuach, M. Preul, A. M. Kinsey, A. N. DeMaria, N. Dib, K. L. Christman, Safety and Efficacy of an Injectable Extracellular Matrix Hydrogel for Treating Myocardial Infarction. *Sci. Transl. Med.* **5**, 173ra25 (2013).
32. J. Tang, A. Vandergriff, Z. Wang, M. T. Hensley, J. Cores, T. A. Allen, P.-U. Dinh, J. Zhang, T. G. Caranasos, K. Cheng, A regenerative cardiac patch formed by spray painting of biomaterials onto the heart. *Tissue Eng. Part C Methods* **23**, 146–155 (2017).
33. S. Roura, C. Soler-Botija, J. R. Bagó, A. Llucià-Valldeperas, M. A. Férnandez, C. Gálvez-Montón, C. Prat-Vidal, I. Perea-Gil, J. Blanco, Postinfarction functional recovery driven by a three-dimensional engineered fibrin patch composed of human umbilical cord blood-derived mesenchymal stem cells. *Stem Cells Transl. Med.* **4**, 956–966 (2015).
34. G. Paradossi, F. Cavalieri, E. Chiessi, C. Spagnoli, Poly(vinyl alcohol) as versatile biomaterial for potential biomedical applications. *J. Mater. Sci. Mater. Med.* **14**, 687–691 (2003).
35. T. Noguchi, T. Yamamuro, M. Oka, P. Kumar, Y. Kotoura, S.-H. Hyon, Y. Ikada, Poly(vinyl alcohol) hydrogel as an artificial articular cartilage: Evaluation of biocompatibility. *J. Appl. Biomater.* **2**, 101–107 (1991).
36. S. Li, X.-H. Yang, Fabrication and characterization of electrospun wool keratin/poly(vinyl alcohol) blend nanofibers. *Adv. Mater. Sci. Eng.* **2014**, 163678 (2014).
37. M.-C. Chen, Z.-W. Lin, M.-H. Ling, Near-infrared light-activatable microneedle system for treating superficial tumors by combination of chemotherapy and photothermal therapy. *ACS Nano* **10**, 93–101 (2016).
38. A. S. Hickey, N. A. Peppas, Mesh size and diffusive characteristics of semicrystalline poly(vinyl alcohol) membranes prepared by freezing/thawing techniques. *J. Membr. Sci.* **107**, 229–237 (1995).
39. C. M. Hassan, J. H. Ward, N. A. Peppas, Modeling of crystal dissolution of poly(vinyl alcohol) gels produced by freezing/thawing processes. *Polymer* **41**, 6729–6739 (2000).
40. C. E. Macias, H. Bodugoz-Senturk, O. K. Muratoglu, Quantification of PVA hydrogel dissolution in water and bovine serum. *Polymer* **54**, 724–729 (2013).
41. K. Cheng, A. Ibrahim, M. T. Hensley, D. Shen, B. Sun, R. Middleton, W. Liu, R. R. Smith, E. Marbán, Relative roles of CD90 and c-Kit to the regenerative efficacy of cardiosphere-derived cells in humans and in a mouse model of myocardial infarction. *J. Am. Heart Assoc.* **3**, e001260 (2014).
42. K. Cheng, K. Malliaras, R. R. Smith, D. Shen, B. Sun, A. Blusztajn, Y. Xie, A. Ibrahim, M. A. Aminzadeh, W. Liu, T.-S. Li, M. A. De Robertis, L. Marbán, L. S. C. Czer, A. Trento, E. Marbán, Human cardiosphere-derived cells from advanced heart failure patients exhibit augmented functional potency in myocardial repair. *JACC Heart Fail.* **2**, 49–61 (2014).
43. Y. Lu, A. A. Aimetti, R. Langer, Z. Gu, Bioresponsive materials. *Nat. Rev. Mater.* **2**, 16075 (2016).
44. N. A. Peppas, A. Khademhosseini, Make better, safer biomaterials. *Nature* **540**, 335–337 (2016).
45. J. Tang, T. Su, K. Huang, P.-U. Dinh, Z. Wang, A. Vandergriff, M. T. Hensley, J. Cores, T. Allen, T. Li, E. Sproul, E. Mihalko, L. J. Lobo, L. Ruterbories, A. Lynch, A. Brown, T. G. Caranasos, D. Shen, G. A. Stouffer, Z. Gu, J. Zhang, K. Cheng, Targeted repair of heart injury by stem cells fused with platelet nanovesicles. *Nat. Biomed. Eng.* **2**, 17–26 (2018).
46. Y. Ye, C. Wang, X. Zhang, Q. Hu, Y. Zhang, Q. Liu, D. Wen, J. Milligan, A. Bellotti, L. Huang, G. Dotti, Z. Gu, A melanin-mediated cancer immunotherapy patch. *Sci. Immunol.* **2**, eaan5692 (2017).
47. L. Luo, J. Tang, K. Nishi, C. Yan, P.-U. Dinh, J. Cores, T. Kudo, J. Zhang, T.-S. Li, K. Cheng, Fabrication of synthetic mesenchymal stem cells for the treatment of acute myocardial infarction in mice. *Circ. Res.* **120**, 1768–1775 (2017).
48. A. Vandergriff, K. Huang, D. Shen, S. Hu, M. T. Hensley, T. G. Caranasos, L. Qian, K. Cheng, Targeting regenerative exosomes to myocardial infarction using cardiac homing peptide. *Theranostics* **8**, 1869–1878 (2018).
49. K. Cheng, K. Malliaras, D. Shen, E. Tseliou, V. Ionta, J. Smith, G. Galang, B. Sun, C. Houde, E. Marbán, Intramyocardial injection of platelet gel promotes endogenous repair and augments cardiac function in rats with myocardial infarction. *J. Am. Coll. Cardiol.* **59**, 256–264 (2012).
50. K. Md. M. Hasan, N. Tamanna, Md. A. Haque, Biochemical and histopathological profiling of Wistar rat treated with *Brassica napus* as a supplementary feed. *Food Sci. Hum. Wellness* **7**, 77–82 (2018).
51. L. E. Lillie, N. J. Temple, L. Z. Florence, Reference values for young normal Sprague–Dawley rats: Weight gain, hematology and clinical chemistry. *Hum. Exp. Toxicol.* **15**, 612–616 (1996).
52. J. Tang, X. Cui, T. G. Caranasos, M. T. Hensley, A. C. Vandergriff, Y. Hartanto, D. Shen, H. Zhang, J. Zhang, K. Cheng, Heart repair using nanogel-encapsulated human cardiac stem cells in mice and pigs with myocardial infarction. *ACS Nano* **11**, 9738–9749 (2017).

Acknowledgments: We thank J. Cores for proofreading the manuscript. **Funding:** This work was supported by the National Institute of Health HL123920 and HL137093, the Sloan Research Fellowships, the NC State University Chancellor's Faculty Excellence Program, and the University of North Carolina General Assembly Research Opportunities Initiative grant. **Author contributions:** J.T., J.W., K.H., Y.Y., Z.G., and K.C. designed the research. J.T., J.W., K.H., and Y.Y. performed the biochemical, cellular, and animal experiments; analyzed the data; and drafted the paper. M.T.H., T.S., L.Q., and T.G.C. performed cellular and in vitro experiments. J.T., J.W., K.H., and Y.Y. contributed equally. J.Z., Z.G., and K.C. directed the research and provided financial support. **Competing interests:** The authors declare that they have no competing interests. **Data and materials availability:** All data needed to evaluate the conclusions in the paper are present in the paper and/or the Supplementary Materials. Additional data related to this paper may be requested from the authors.

Submitted 23 April 2018
Accepted 26 October 2018
Published 28 November 2018
10.1126/sciadv.aat9365

Citation: J. Tang, J. Wang, K. Huang, Y. Ye, T. Su, L. Qiao, M. T. Hensley, T. G. Caranasos, J. Zhang, Z. Gu, K. Cheng, Cardiac cell–integrated microneedle patch for treating myocardial infarction. *Sci. Adv.* **4**, eaat9365 (2018).